

ornl

**OAK RIDGE
NATIONAL
LABORATORY**

MARTIN MARIETTA

OPERATED BY
MARTIN MARIETTA ENERGY SYSTEMS, INC.
FOR THE UNITED STATES
DEPARTMENT OF ENERGY



3 4456 0004609 1

ORNL/TM-9893

**Toroidal Field Effects
on the Stability on the Heliotron E**

B. A. Carreras
L. Garcia
V. E. Lynch

OAK RIDGE NATIONAL LABORATORY
CENTRAL RESEARCH LIBRARY
CIRCULATION SECTION
ROOM 1001
LIBRARY LOAN COPY
DO NOT TRANSFER TO ANOTHER PERSON
If you wish someone else to see this
report, send in name with report and
the library will arrange a loan.

Printed in the United States of America. Available from
National Technical Information Service
U.S. Department of Commerce
5285 Port Royal Road, Springfield, Virginia 22161
NTIS price codes—Printed Copy: A03; Microfiche A01

This report was prepared as an account of work sponsored by an agency of the United States Government. Neither the United States Government nor any agency thereof, nor any of their employees, make any warranty, express or implied, or assumes any legal liability or responsibility for the accuracy, completeness, or usefulness of any information, apparatus, product, or process disclosed, or represents that its use would not infringe privately owned rights. Reference herein to any specific commercial product, process, or service by trade name, trademark, manufacturer, or otherwise, does not necessarily constitute or imply its endorsement, recommendation, or favoring by the United States Government or any agency thereof. The views and opinions of authors expressed herein do not necessarily state or reflect those of the United States Government or any agency thereof.

ORNL/TM-9893
Dist. Category UC-20g

Fusion Energy Division

TOROIDAL FIELD EFFECTS ON THE STABILITY OF HELIOTRON E

B. A. Carreras and L. Garcia
Fusion Energy Division

V. E. Lynch
Computing and Telecommunications Division

Date Published - February 1986

Prepared by
OAK RIDGE NATIONAL LABORATORY
Oak Ridge, Tennessee 37831
operated by
MARTIN MARIETTA ENERGY SYSTEMS, INC.
for the
U.S. DEPARTMENT OF ENERGY
under Contract No. DE-AC05-84OR21400



3 4456 0004609 1

CONTENTS

ABSTRACT.....	v
I. INTRODUCTION.....	1
II. STELLARATOR EXPANSION EQUATIONS.....	3
III. HELIOTRON E STABILITY RESULTS.....	8
IV. THE EFFECTS OF ADDITIONAL TOROIDAL FIELD ON THE STABILITY OF HELIOTRON E.....	13
V. RESISTIVE INSTABILITIES.....	24
VI. CONCLUSIONS.....	26
REFERENCES.....	29

ABSTRACT

The addition of a small toroidal field to the Heliotron E configuration improves the stability of the $n=1$ mode and increases the value of the stability beta critical. Total stabilization of this mode can be achieved with added toroidal fields between 5 and 15% of the total field. In this situation, the plasma can have direct access to the second stability regime. For the Heliotron E configuration, the self-stabilization effect is due to the shear, not to the magnetic well. The toroidal field threshold value for stability depends strongly on the pressure profile and the plasma radius.

I. INTRODUCTION

For stellarators with large aspect ratio, the most reasonable way to improve their stability properties is to rely on the beta self-stabilization effect¹ and find a stable path to the second stability regime. In general, this implies the need for external control of the rotational transform profile. Such control can be achieved by a system of poloidal field coils.^{2,3} This method is now being implemented in the Advanced Toroidal Facility (ATF) device.⁴ As we show, an alternative way is the combination of slow heating and the use of the toroidal field coils which are characteristic of the Heliotron configurations.⁵

We have studied the effect of the added toroidal field on the stability of a configuration that models Heliotron E.⁶ Calculations⁷⁻¹⁰ of low n mode stability for this configuration give beta limits that range from 1.4 to 2%, depending on the pressure profile. These theoretical predictions are compatible with the present experimental results.¹¹ Due to the high rotational transform, Heliotron E has a very high equilibrium beta limit. Therefore, as a beta optimization implies possible trade-offs between equilibrium and stability properties, in the case of Heliotron E there is room enough for optimization of the overall beta limit. In Heliotron E high-beta operation, no use has yet been made of the toroidal field coils, which can greatly change the range of the rotational transform.¹² It is of great interest to find out if its present beta capability can be improved by the use of those coils.

The effect of the toroidal field is quite important. The addition of a modest toroidal field (a small percentage of the total field) moves the $\iota=1$ surface to a region of high shear. The increase of shear stabilizes the $(m=1;n=1)$ mode, which is the most unstable mode for the Heliotron E. Due to this stabilizing effect, the critical beta increases with increasing toroidal field. Moreover, if the toroidal field is large enough (from 5 to 15% of the total field), the $n=1$ mode is totally stabilized, and the plasma can gain stable access to the second stability regime. The threshold value of the toroidal field for

the total stabilization of the $n=1$ mode depends strongly on the pressure profile and minor radius of the plasma. This stabilization effect is operative for zero-current equilibria but is not effective for flux-conserving equilibria. Therefore, in Heliotron E, slow heating should be more efficient than fast heating.

It is interesting to note that the mechanism for the plasma beta self-stabilization is, in this case, very different from the case of ATF. For Heliotron E plasmas, the stabilization is mainly due to the increase of shear at the $\iota=1$ surface, instead of the deepening of the magnetic well. As beta increases, for zero-current equilibrium the transform at the plasma edge decreases, while the transform at the magnetic axis increases. This causes the $\iota=1$ surface to move to a higher shear region.

Since the shear is the dominant stabilizing effect, a weak stabilization can be expected only for the resistive instabilities. This is certainly the case for the linear instability. However, nonlinearly the stabilizing effect is more pronounced, and the saturated level of fluctuations decreases with the added toroidal field. Thus, an improvement on confinement at finite-beta can also be expected.

In this paper, we present the results of these studies. In Sec. II, the equations and methods used are discussed. The numerical results for the standard Heliotron E configuration are presented in Sec. III. In Sec. IV, the results for the toroidal field effects on the stability are discussed. Modification of these effects due to the finite resistivity of the plasma is considered in Sec. V. Finally, in Sec. VI, our conclusions are presented.

II. STELLARATOR EXPANSION EQUATIONS

The studies presented in this paper are based on the stellarator expansion^{1,13} approach to equilibrium and stability of three-dimensional configurations. For planar axis configurations with pitch parameter, $p = M/lA_c$ (where l is the poloidal multipolarity, M is the number of toroidal field periods, and A_c is the coil aspect ratio), close to the pitch value of the Heliotron E, the stellarator expansion compares favorably with three-dimensional calculations.^{2,14} Therefore, it is a useful approach for magnetohydrodynamic (MHD) studies.

The stellarator expansion reduces the equilibrium problem to the solution of a Grad-Shafranov type equation,

$$\Delta^* \psi = -R^2 \frac{dp}{d\psi} - (F + F^*) \frac{dF}{d\psi} + \Delta^* \psi_v^* \quad (1)$$

for the average poloidal flux function ψ . Here the average pressure p and the $F = RB_\zeta$ are only functions of ψ . The average poloidal flux function for the vacuum configuration is ψ_v^* . We follow here the same notation as in Ref. 2, where all the equations and their derivation are discussed in detail. The effect of the average helical curvature is included in the F^* term, which is given by

$$F^* = -\frac{R^2}{F} \langle |\vec{\nabla} \tilde{\chi}|^2 \rangle, \quad (2)$$

where $\tilde{\chi}$ is the magnetostatic potential of the toroidally varying magnetic field, $B_v = \vec{\nabla} \tilde{\chi}$, the brackets $\langle \rangle$ indicate an average over the toroidal angle ζ ,

$$\langle f \rangle = \frac{1}{2\pi} \int_0^{2\pi} f \, d\zeta, \quad (3)$$

and the tilde (\sim) denotes toroidally varying quantities. Therefore, $\langle \tilde{X} \rangle = 0$.

Equation (1) is solved numerically by the RSTEQ¹⁵ equilibrium code. The input is the vacuum magnetic field data, F^* and ψ_v^* , and a given pressure profile $p(\psi)$. The equation is solved either by requiring zero toroidal current in each flux surface or by specifying a rotational transform profile. In particular, the prescribed rotational transform profile can be that of the vacuum configuration, in which case the equilibrium is called flux conserving.

The reduced MHD equations for stellarator configurations were derived¹⁶ by extending the stellarator expansion to the dynamical evolution problem. They are

$$\frac{\partial \psi}{\partial t} + \vec{v}_\perp \cdot \vec{\nabla} \psi = -B_0 \frac{\partial \phi}{\partial \zeta} + R\eta J_\zeta, \quad (4)$$

$$\rho_m \left(\frac{\partial U}{\partial t} + \vec{v}_\perp \cdot \vec{\nabla} U \right) = \frac{1}{R} \hat{\zeta} \cdot \left(\vec{\nabla} J_\zeta \times \vec{\nabla} \psi \right) - \frac{B_0}{R} \frac{\partial J_\zeta}{\partial \zeta} + \hat{\zeta} \cdot \left(\vec{\nabla} \times \Omega \vec{\nabla} p \right), \quad (5)$$

and

$$\frac{\partial p}{\partial t} + \vec{v}_\perp \cdot \vec{\nabla} p = 0, \quad (6)$$

with

$$\Omega = \frac{R^2}{R_0^2} - 1 - \frac{F^*}{B_0 R_0}, \quad (7)$$

where $\vec{\nabla}\Omega$ is the average curvature, the toroidal current density is

$$J_{\zeta} = \frac{1}{R} \Delta^* (\psi - \psi_v^*), \quad (8)$$

the vorticity in the toroidal direction is

$$U = \nabla_{\perp}^2 \phi, \quad (9)$$

and the poloidal velocity is

$$\vec{V}_{\perp} = \vec{\nabla}\phi \times \hat{\zeta}. \quad (10)$$

The vorticity and the velocity are expressed in terms of the stream function ϕ .

Here, R_0 is the major radius and B_0 the vacuum toroidal field at $R = R_0$. S is the ratio between the resistive time and the poloidal Alfvén time. The last term in Eq. (4) is nonzero only when resistive effects are included in the calculation (see Sec. V).

This system of equations is solved by the implicit code FAR.¹⁷ Equilibrium flux coordinates (ρ, θ, ζ) are used. Here, ρ is a generalized radial variable defined by $\phi = B_0 \rho^2 / 2$, where ϕ is the toroidal flux function. Hereafter, the coordinate ρ will be normalized to its value at the plasma edge. The code uses finite differences in the radial direction and Fourier expansion in the two angular variables, and can be used for linear or nonlinear calculations. The numerical scheme is fully implicit for the linear terms.

All results in this paper are from fixed boundary equilibrium and stability calculations, in which only low n modes have been considered. Because the instabilities investigated here are basically interchange modes highly localized in radius, careful convergence studies are essential. The smallest radial mesh size used in the present calculations is $\Delta\rho = 1.25 \times 10^{-3}$. It is interesting to note that for instabilities close to marginal point, the sensitivity to the radial

mesh size is higher than was expected. We calculated linear growth rates for several radial meshes with fewer than 100 grid points and extrapolated the results to zero mesh size using a polynomial in $\Delta\rho$ with coefficients calculated by a least-squares fit to the calculated growth rates [Fig. 1(a)]. For the particular case $p \propto \psi^4$, shown in Fig. 1, the extrapolation gives $\gamma = 1.104 \times 10^{-2} \tau_{hp}^{-1}$. Repeating the

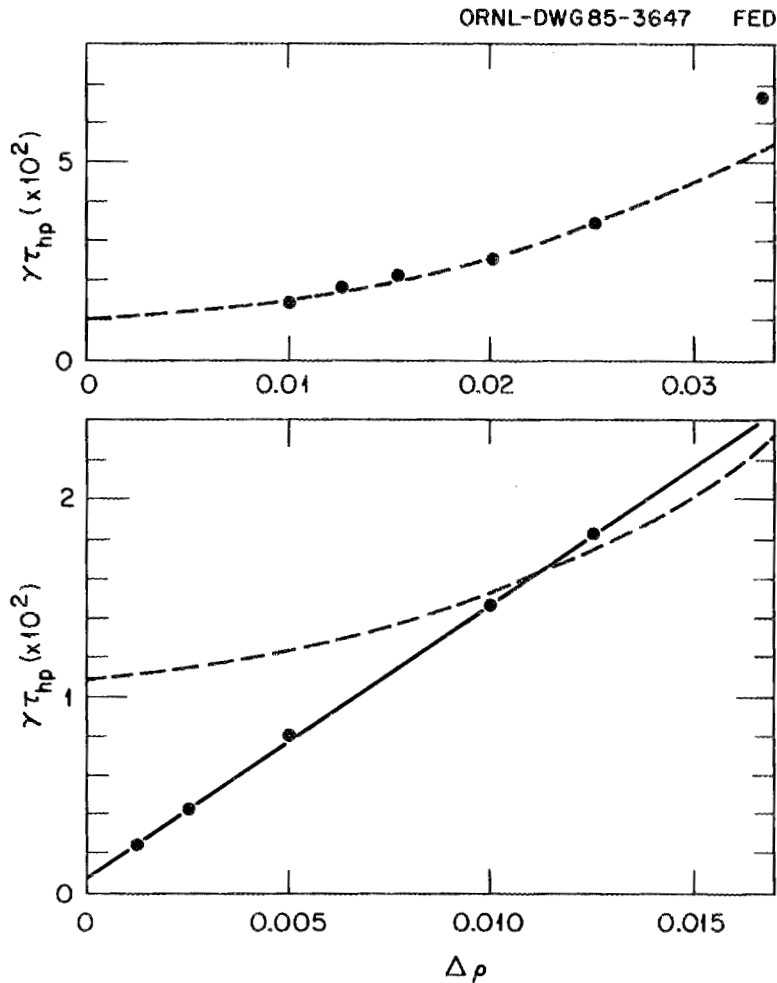


FIG. 1. Comparison between the extrapolation by a least-squares fit to the numerical linear growth with (a) grids of less than 100 points (broken line) with (b) to grids with more than 100 grid points (continuous line). The case with 30 grid points has not been included in the least-squares fit.

convergence calculation with radial grids between 80 and 800 grid points [Fig. 1(b)] yields an extrapolated growth rate $\gamma = 4.712 \times 10^{-4} \tau_{hp}^{-1}$. There is more than an order of magnitude variation between the two extrapolated values. This is a systematic effect, which suggests that caution should then be taken in evaluating the results of stability calculations based on radial grids with fewer than 100 grid points. The growth rates are less sensitive to the toroidally coupled modes. In our calculations, for a given toroidal mode number n , we include about 10 poloidal components. However, it is possible to obtain quite accurate results with half this number in most cases. All of these numerical requirements are clearly a consequence of the nature of the instability. They underline that the modes are essentially interchange modes.

The resistive stability calculations do not require such fine radial grids. For the nonlinear, single-helicity calculations, 400 radial grid points were used, and harmonics from the (1;1) to the (12;12) were included. Further numerical details on the whole approach are given in Ref. 18.

III. HELIOTRON E STABILITY RESULTS

The Heliotron E device basically consists of a $l = 2$ helical coil with $M = 19$ toroidal field periods. The plasma aspect ratio for the standard configuration is $A_p = 10$, and the average plasma minor radius, $\bar{a} = 20$ cm. The configuration also has toroidal field coils, providing an extra degree of flexibility to the device with effects we study in Sec. IV. For the present studies, the vacuum field has been calculated with a single filament coil model.¹⁸ The minor radius of the filamentary helical coil, $a_H = 0.32$ m, has been adjusted to yield the same transform values as does the finite-size coil model.¹² The high aspect ratio and number of field periods cause the rotational transform to be high ($\iota = 0.5$) at the magnetic axis and $\iota = 2.3$ at the plasma edge for the standard configuration. In this section, we consider the equilibrium and stability properties of this standard configuration.

Due to the large rotational transform, the plasma equilibrium beta limit is high. If we take the conventional definition of equilibrium beta critical as the value of beta at which the magnetic axis shift is one-half of the plasma radius, we obtain a peak beta critical value for Heliotron E of about 20%. In Fig. 2 the magnetic axis shift as a function of beta is plotted for different equilibrium conditions. The volume-averaged equilibrium beta critical depends on the pressure profile (from $\langle\beta\rangle = 5\%$ to $\langle\beta\rangle = 9\%$) and on whether the equilibrium is constrained to be flux conserving or zero current.

In comparing our results with previous calculations of Heliotron equilibrium and stability, it is important to discuss in detail the question of pressure profile dependence. We have parameterized the pressure profile in the following way:

$$p_f(\rho) = p(0) \left[\frac{f(1) - f(\rho)}{f(1) - f(0)} \right]^{\alpha_f}, \quad (11)$$

where f is a flux function. In particular, f can be the poloidal flux function, ψ , or the toroidal flux function, Φ . The exponent α_f is in

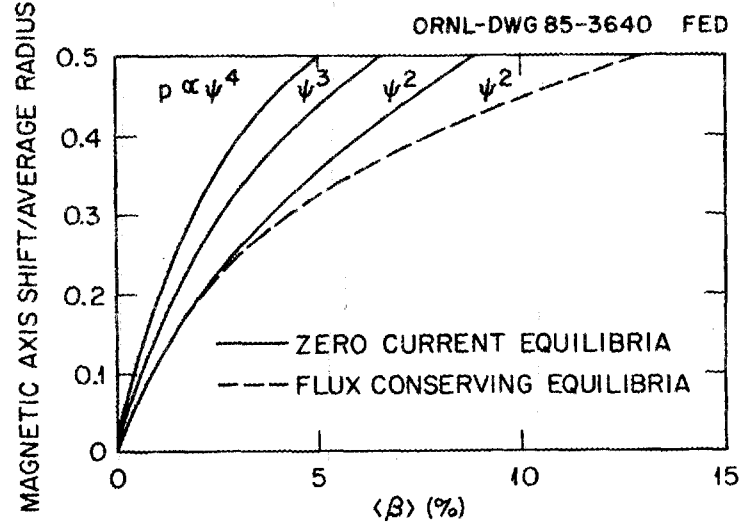


FIG. 2. Magnetic axis shift versus average beta for the Heliotron E configuration. The results from different pressure profiles and zero-current equilibria are plotted with a continuous line. The broken line is for a $p \propto \psi^2$ profile, flux-conserving equilibrium.

general an integer, but noninteger values have also been considered. Parameterizations of this type are often used, and commonly f is taken to be the toroidal flux function or ρ^2 , which by definition is equivalent. For simplicity, we denote the pressure profile given by Eq. (11) as $p \propto f^{\alpha_f}$. In comparing results for pressure profiles with $f = \psi$ with pressure profiles with $f = \psi^2$, note that, at the magnetic axis

$$\frac{dp_\psi}{d\rho} = \frac{2\alpha_\psi}{\alpha_\psi} \frac{1}{\psi(0)} \frac{dp_\psi}{d\rho} \int_0^1 \rho d\rho \psi(\rho). \quad (12)$$

Therefore, for both profiles to be the same near the axis, we require

$$\alpha_\psi \psi(0) = 2\alpha_\psi \int_0^1 \rho d\rho \psi(\rho). \quad (13)$$

In particular, for Heliotron E near the magnetic axis, the profile $p \propto \psi^2$ is close to the profile $p \propto \Phi$ (Fig. 3). However, near the $\iota=1$ surface they are rather different. We can expect these two profiles to lead to similar magnetic axis shifts but to have very different stability properties for the $(m=1;n=1)$ mode. Because most of the previous stability calculations have been done for pressure profiles proportional to a power of the toroidal flux, we study here the case of profiles proportional to a power of the poloidal flux.

For the standard Heliotron E configuration, the most unstable mode is the $(m=1;n=1)$, which is resonant at the $\iota=1$ surface. The linear instability threshold for the $p \propto \psi^2$ profile is at the $\langle \beta \rangle \approx 1.4\%$, and the $m=1$ component of the $n=1$ mode is clearly the dominant one. This result agrees well with previous stability calculations.⁷⁻⁹ In Fig. 4,

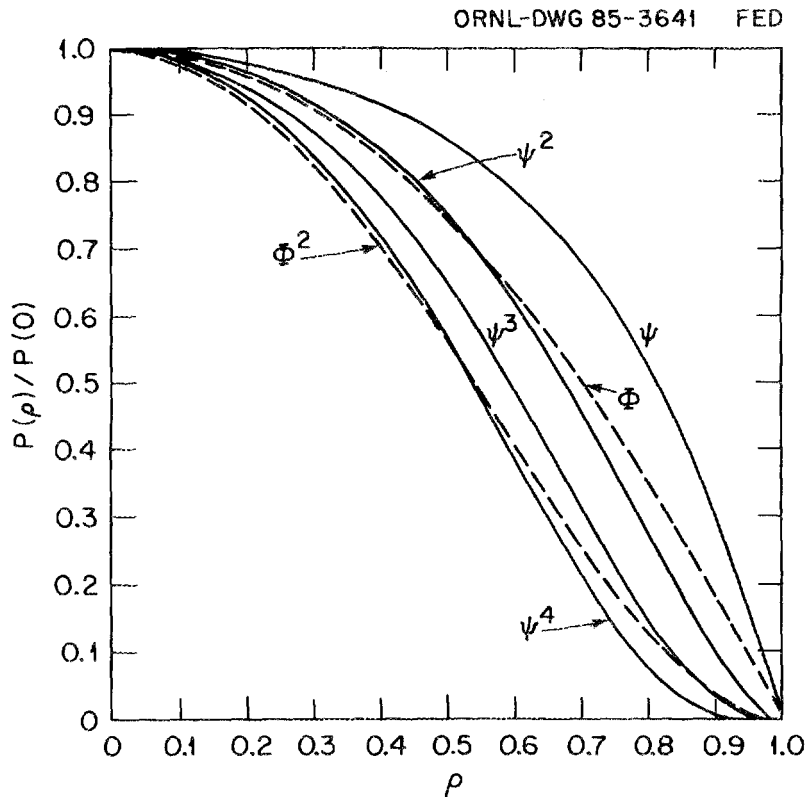


FIG. 3. Profiles proportional to different powers of the average poloidal flux ψ and toroidal flux Φ .

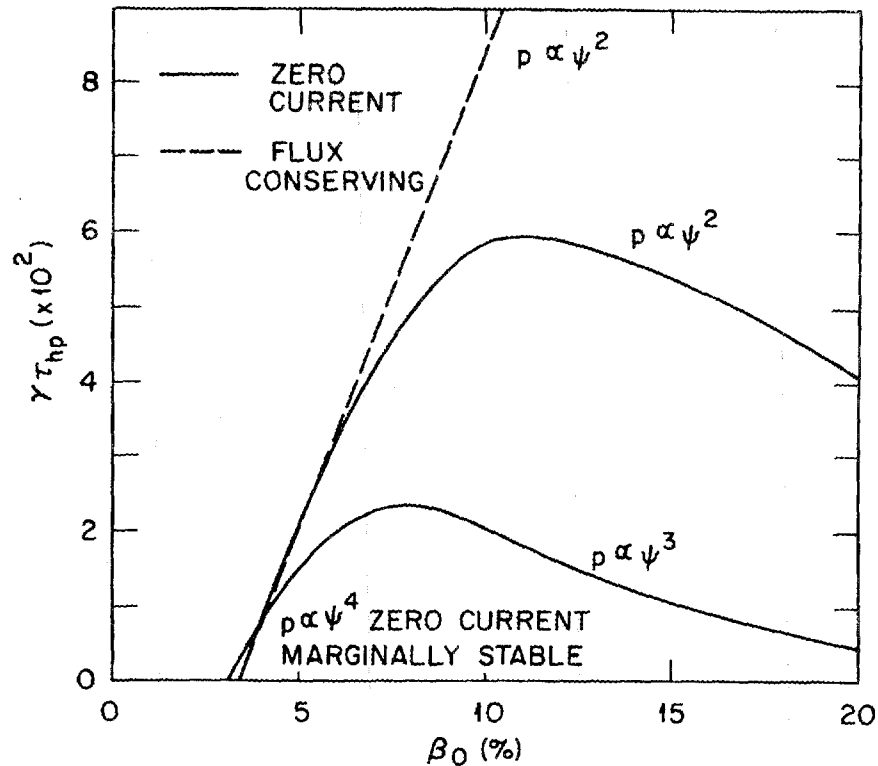


FIG. 4. Linear growth rate of the $n=1$ mode versus peak beta for different pressure profiles. The results for zero-current equilibria (continuous line) are contrasted with the results from flux-conserving equilibria (broken line).

we have summarized the results for different pressure profiles, plotting the linear growth rate as a function of beta. As the profile becomes more peaked at the center, the gradient of p at the $r=1$ surface decreases and the mode is stabilized. For the $p \propto \psi^4$ profile, when detailed convergence studies have been performed (see Sec. II), the $n=1$ instability is limited to a very narrow region in beta $1.8\% < \langle \beta \rangle < 3.0\%$ with growth rates below $10^{-3} \tau_{hp}^{-1}$. From a practical point of view, we take the mode to be marginally stable for this profile. In this case, the beta limit is then given by the equilibrium beta limit, which is $\langle \beta \rangle \approx 5\%$.

There is no difference in the instability threshold for a zero-current and a flux-conserving equilibrium. However, the latter gives higher growth rates for betas above the threshold value. Moreover, for the flux-conserving equilibrium, there is no indication of beta self-stabilization effect, which is quite apparent for the zero-current case. Similar behavior has been found by M. Wakatani¹⁹ using the three-dimensional stability code BETA.²⁰ The second stability regime for the broader profiles is beyond the beta values for which we are able to get converged equilibria. For the more peaked profiles, this is not the case, and as noted above for the $p \propto \psi^4$ profile, the first and second stability regions merge and the instability is marginal. Therefore, it is extremely important for the stability of the $n=1$ to have both a slow heating system (maintaining zero current) and a favorable pressure profile. Long pulse heating and the right combination of gas puffing and pellet injection could lead to remarkable improvements in the high-beta performance of Heliotron E. We postpone the detailed study of the beta self-stabilization mechanism to Sec. VI.

IV. THE EFFECT OF ADDITIONAL TOROIDAL FIELD ON THE STABILITY OF HELIOTRON E

We have added 19 circular toroidal field coils to the standard Heliotron E model described in Sec. III. They are located at the beginning of each field period. The radius of these coils is $a_T = 0.59$ m. The toroidal field ripple caused by these coils does not affect the flux surfaces, at least for the range of toroidal fields considered here, up to 15% of the total toroidal field.

Adding the external toroidal field to the toroidal field generated by the helical coils reduces the rotational transform, and the plasma minor radius increases. In general, we have assumed that a limiter is used in such a way that the plasma aspect ratio is kept constant, but we also have studied the effect of changing the limiter position. The decrease of rotational transform is illustrated in Fig. 5, where the rotational transforms at the magnetic axis and at the plasma edge are plotted versus the relative magnitude of the added toroidal field, B_T/B_0 . The change of $\iota(0)$ with B_T/B_0 agrees well with that calculated analytically using the stellarator expansion and a simple Bessel function model for the vacuum helical field, which gives

$$\iota(0) = \frac{M\delta^2}{4} \frac{1}{(1 + B_T/B_0)^2} = \frac{\iota_0}{(1 + B_T/B_0)^2}, \quad (14)$$

where $\delta = \frac{3}{|B_v|/B_0}$ and ι_0 is the transform at the magnetic axis for the standard configuration.

The reduction of the rotational transform with the added toroidal field results in an increase in the magnetic axis shift at finite beta. In Fig. 6 the magnetic axis shift for the standard configuration is compared with a case with $B_T/B_0 = 0.15$. The larger shift gives a deeper magnetic well, as can be seen in the same figure. The minimum of $[V'(\rho) - V'(0)]/V'(0)$ is also plotted as a function of beta for the same two configurations. Here, V' is the derivative of the volume

ORNL-DWG85-3650 FED

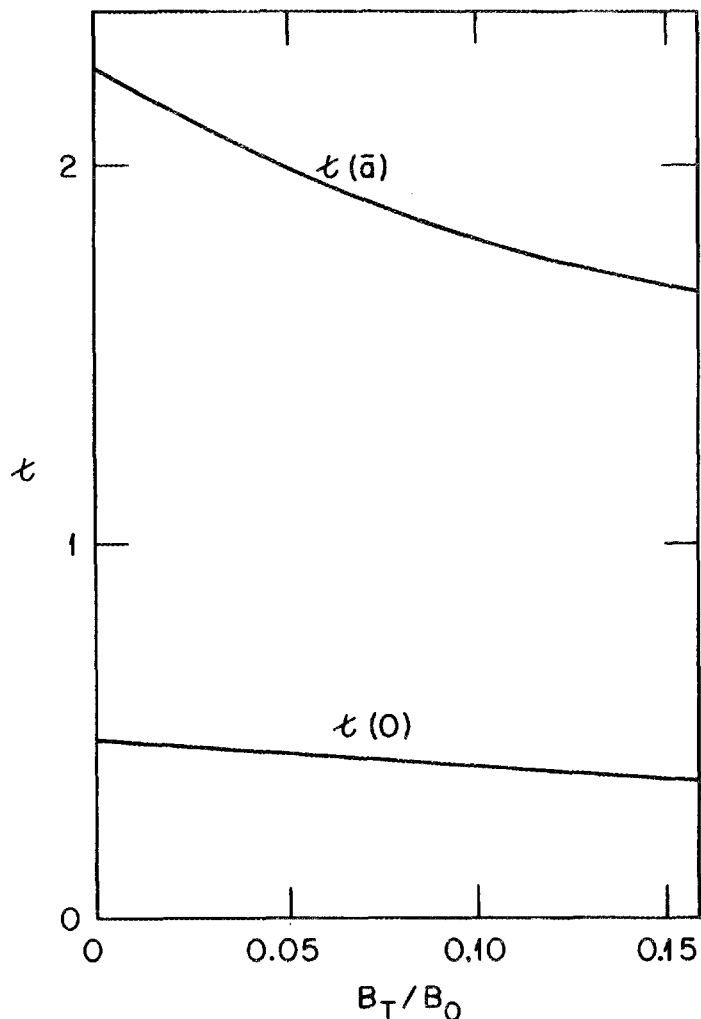


FIG. 5. Change of the rotational transform at the magnetic axis and at the plasma edge with the addition of toroidal field.

enclosed by a flux surface with respect to the toroidal flux. Therefore, with modest toroidal fields the Heliotron E configuration gains a great deal of flexibility and control on the physics parameters relevant for equilibrium and stability of the plasma.

The stability properties of the $n=1$ mode are very sensitive to the magnitude of the added toroidal field. In Fig. 7, we have plotted the linear growth rate of the $n=1$ mode as a function of peak beta for

ORNL-DWG 85-3643 FED

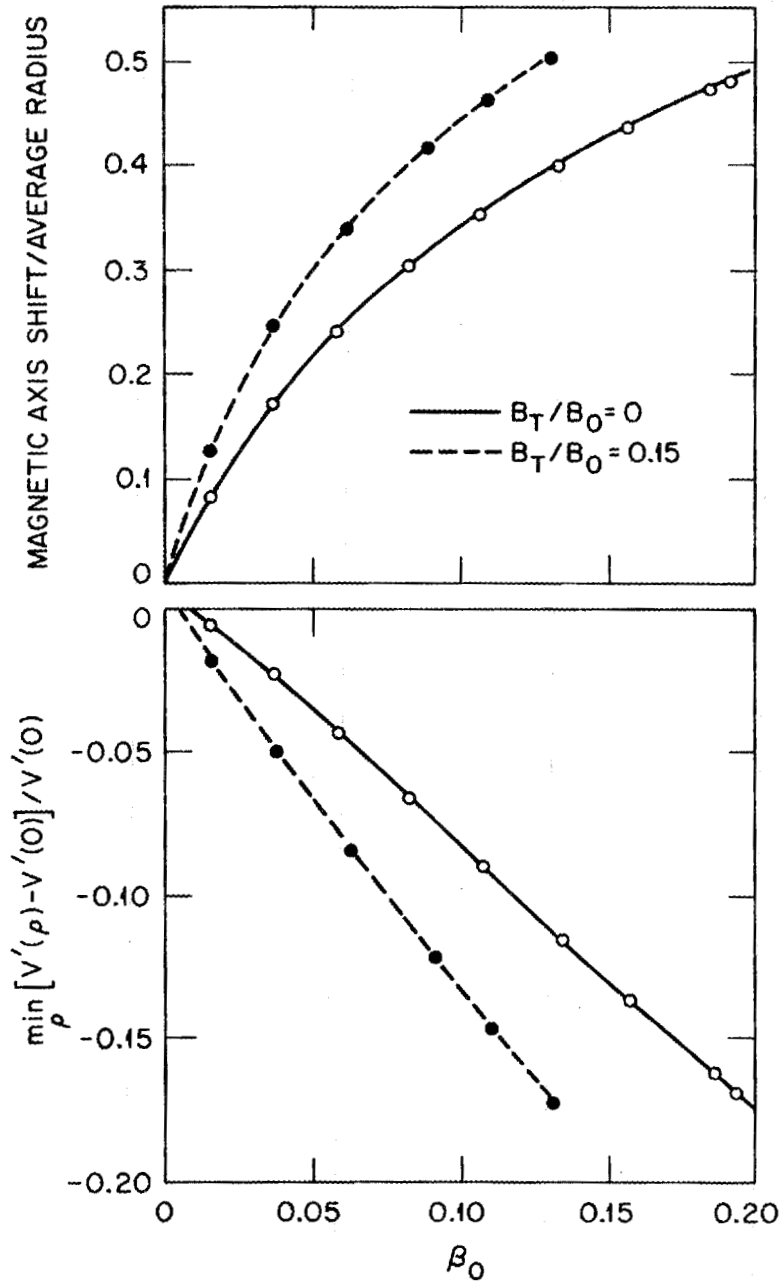


FIG. 6. Magnetic axis shift and magnetic well depth as a function of beta for the standard Heliotron E configuration and for the case with a 15% additional toroidal field. The results are for a zero-current equilibrium with pressure profile $p \propto \psi^2$.

different values of the toroidal field. These calculations were done for zero-current equilibria with a pressure profile $p \propto \psi^2$. When the added toroidal field is 15% of the total field, the $n=1$ mode is stable. As in the case of the standard Heliotron E configuration, the dominant component of the $n=1$ mode is the $(m=1;n=1)$. This component, for beta values near the threshold, is very localized in the radial direction (Fig. 8). It is then reasonable to assume that the stability properties of the mode depend mostly on local quantities at the $\iota=1$ surface. For a constant beta value, we can plot the local shear and value of the V'' as a function of B_T/B_0 (Fig. 9). We can see that as the linear growth rate decreases, the shear increases, while V'' becomes increasingly positive. There is also a small decrease on the local pressure gradient as the $\iota=1$ surface moves outward. Therefore, since the overall effect is stabilizing, the shear stabilization has to dominate. In fact, as the toroidal field increases, the $\iota=1$ surface moves towards a higher shear region, and the shear effect is strong enough to stabilize the mode.

As the $n=1$ mode is stabilized by the effect of the toroidal field, the critical stability beta for this mode becomes higher. All these effects have been summarized in Fig. 10, where lines of constant $n=1$ linear growth rate in the beta- B_T plane have been plotted. In this figure also appears the equilibrium beta critical contour (dotted line). For $B_T/B_0 \gtrsim 0.15$, the beta limitation is due only to equilibrium failure. In this situation, peak betas well above 10% could be achieved in the Heliotron E device.

The results shown in Fig. 10 are for a strongly unstable pressure profile, $p \propto \psi^2$. For more favorable profiles, the toroidal field required to stabilize the $n=1$ mode is much smaller. For instance, for the $p \propto \psi^3$ pressure profile only a 5% increase of the toroidal field is required (Fig. 11). In this case, even higher values of beta could be attained in the Heliotron device.

The $n=1$ mode stability is also sensitive to the plasma radius. If we assume that an ideal limiter is used which reduces the plasma size by 10%, the value of the toroidal field required to stabilize this mode

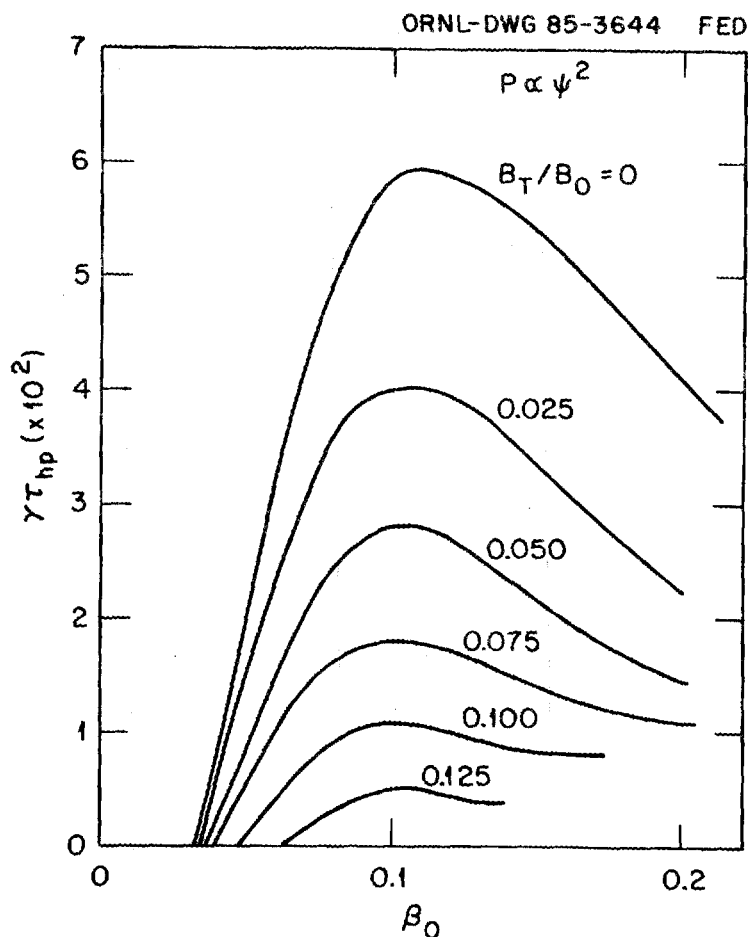


FIG. 7. Linear growth rate versus peak beta for different values of additional toroidal field. All results are for zero-current equilibria with $p \propto \psi^2$ pressure profile.

also is reduced (Fig. 12). This sensitivity is low for the standard Heliotron E configuration but becomes very important when the toroidal field is added.

Internal modes for stellarator configurations, when they are unstable, have growth rates that increase with n . Therefore, we expect higher n modes to have higher growth rate than the $n=1$ mode. However, the numerical results show that their instability threshold is always very close to the $n=1$ mode threshold. We have studied the stability of Heliotron E plasmas to $n=2$ modes with different toroidal fields. The

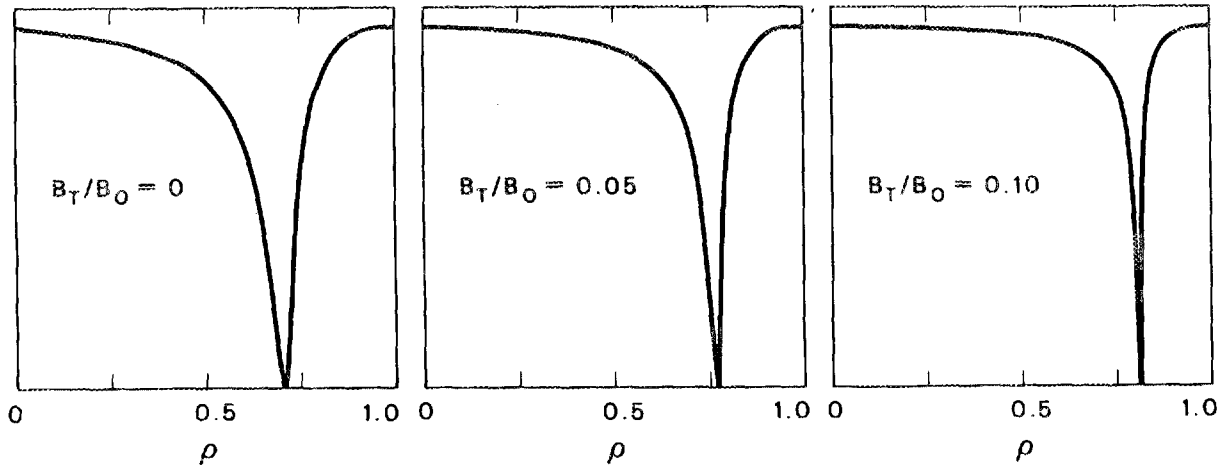


FIG. 8. Change of the $(m=1;n=1)$ component of the $n=1$ mode for zero-current equilibria with peak beta 6% and pressure profile $p \propto \psi^2$ for different toroidal field values. Note that as the toroidal field increases, the instability peak shifts outward and narrows in width.

marginal stability contours in the β_0 - B_T plane (Figs. 10 to 12) are hardly changed by the $n=2$ modes. This can be seen in Fig. 13, where the linear growth rates at fixed β_0 for the $n=1$ and $n=2$ modes are plotted as a function of B_T/B_0 . The instability thresholds for both modes are practically the same. Therefore, the calculated marginal stability contours for the $n=1$ mode can be taken as the marginal stability contours for all n modes.

We now return to the problem of beta self-stabilization. We can see from Figs. 10 to 12 that the self-stabilization effect can be strong enough to totally stabilize the $n=1$ mode and not merely reduce the linear growth rate. From the analysis of the stabilization due to the addition of toroidal field, we have seen that the increase of the shear at the $\iota=1$ surface is probably the cause of the stabilization. This seems to be also the main cause of the beta self-stabilization effect. As beta increases, the transform changes to maintain zero current in each flux surface. In doing so, the transform at the

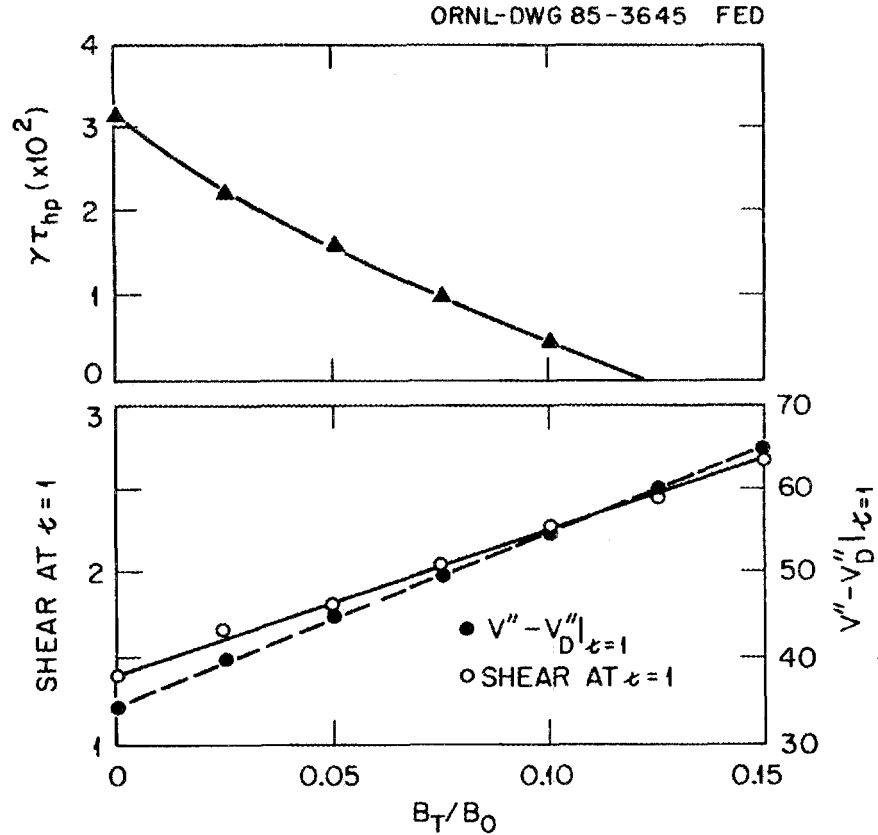


FIG. 9. Linear growth rate for the same toroidal field scan as in Fig. 8. The values of the shear and V'' at the $\iota=1$ surface are also shown.

magnetic axis increases, that at the plasma edge decreases, and the whole profile is strongly distorted. This distortion produces an increase of the shear at the $\iota=1$ surface. As in the case of the addition of a toroidal field, the V'' stays positive and increasing at the $\iota=1$ surface. Therefore, the second stability region in Heliotron E has to be due to shear stabilization and not to the magnetic well. It is also important to notice that as beta increases, the pressure gradient at the singular surface changes. The way it changes depends on the pressure profile (Fig. 14). For the most stable profile, $p \propto \psi^4$, the change is considerably larger than for the $p \propto \psi^2$ profile. This causes the strong differences observed in the stability of the $n=1$ mode.

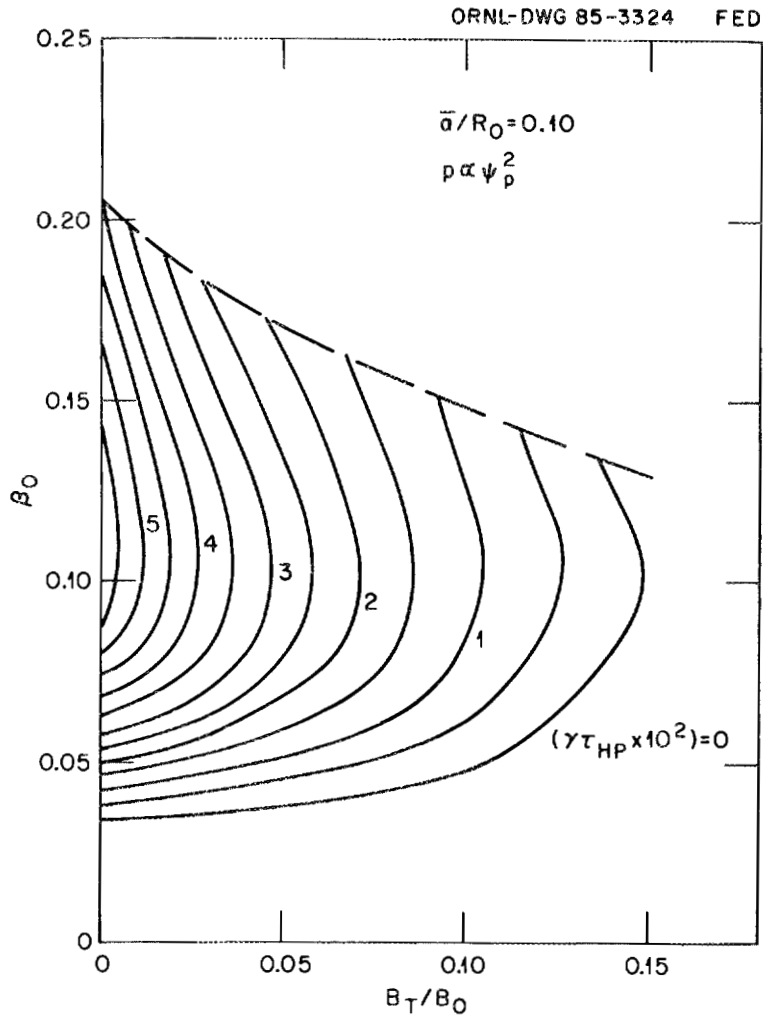


FIG. 10. Constant linear growth rate contour plots in the beta- B_T plane for zero-current equilibria with $p \propto \psi^2$ pressure profile. The broken line is the value of beta for which the magnetic axis shift is one-half the minor radius.

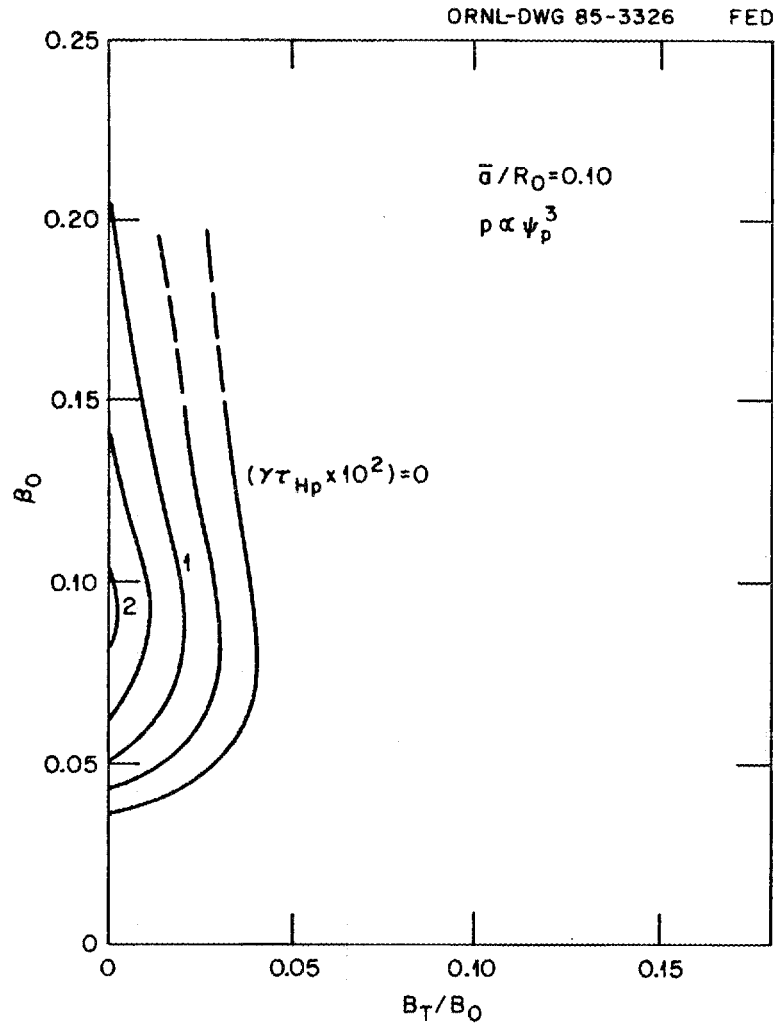


FIG. 11. Same as Fig. 10 for equilibria with pressure profile $p \propto \psi^3$.

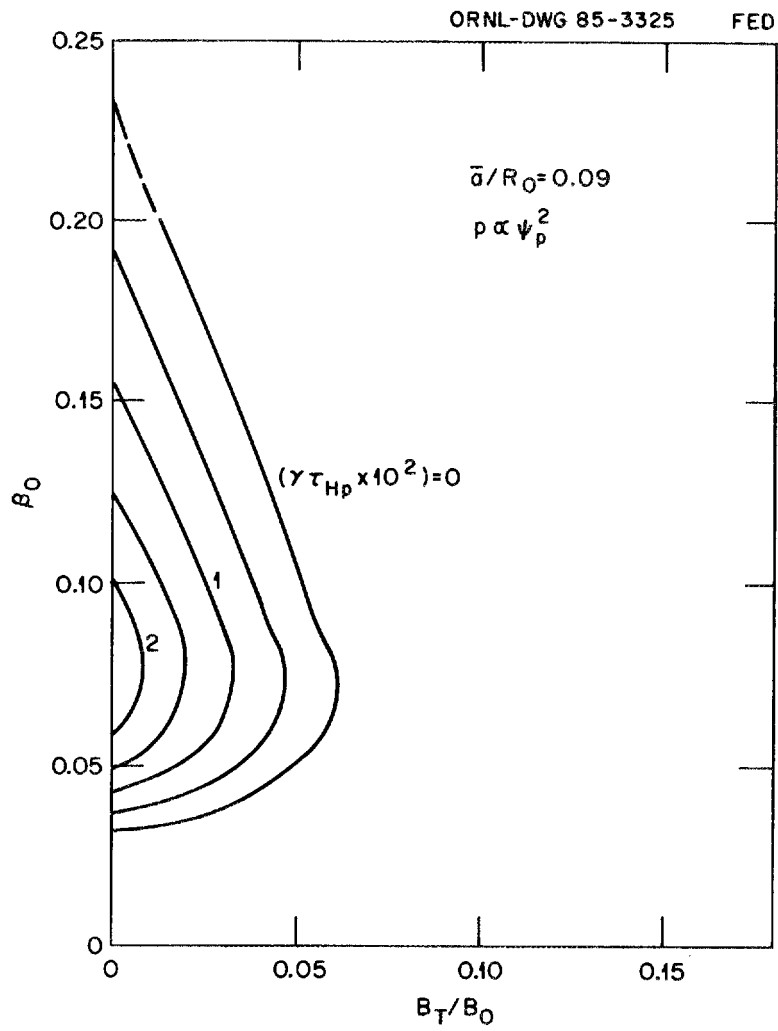


FIG. 12. Same as Fig. 10 for a plasma inverse aspect ratio 0.09.

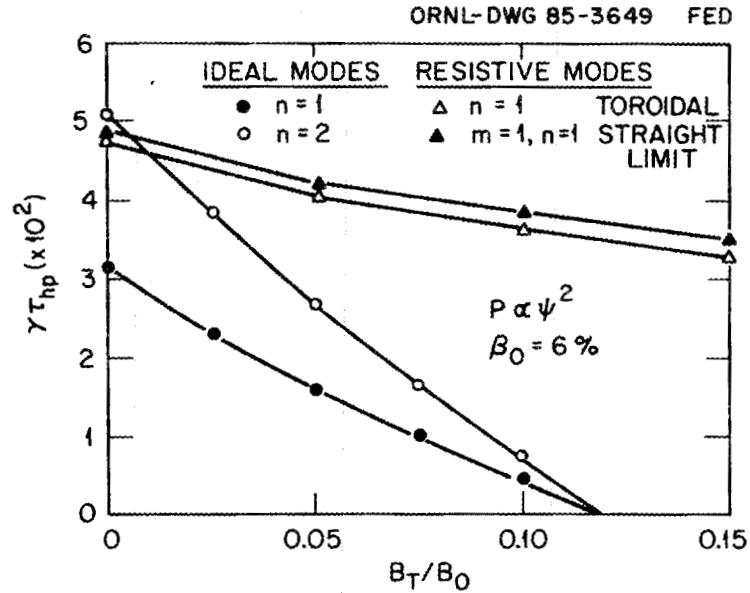


FIG. 13. Linear growth rate of the $n=1$ and $n=2$ modes for the same toroidal field scan as in Fig. 8. The linear growth rate for the resistive $n=1$ mode for $S = 10^5$, and the resistive growth rate of the ($m=1; n=1$) mode in the cylindrical limit are also plotted.

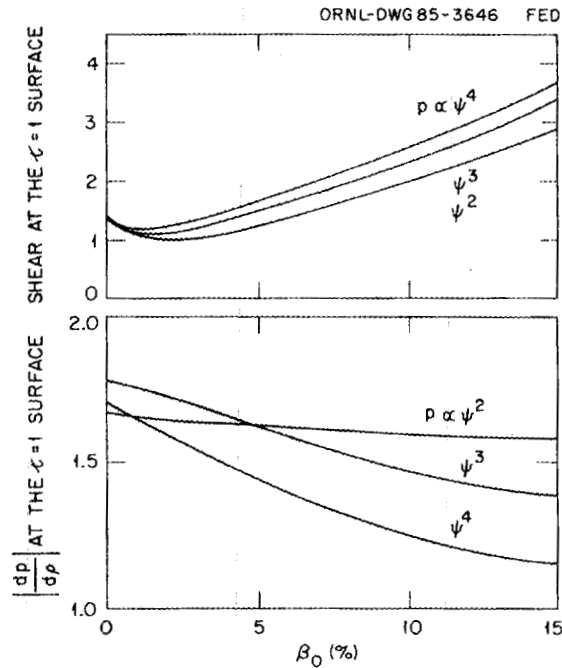


FIG. 14. Change of shear and pressure gradient at the $\iota=1$ surface with β_0 for the standard Heliotron E configuration. The plots are for zero-current equilibria with different pressure profiles.

V. RESISTIVE INSTABILITIES

Because the shear is the dominant stabilizing mechanism for the $n=1$ mode in Heliotron E, it is important to analyze the effect of the resistivity on the instability of this mode. The shear has a strong stabilizing effect on the ideal instabilities, but its effect on the linear growth rate of resistive instabilities is expected to be weak. Therefore, the inclusion of resistivity could greatly modify the picture we have drawn of the stability of Heliotron E and make its experimental verification very difficult.

First, we reexamine the change of linear stability properties due to the added toroidal field. If we calculate the linear growth rate for fixed beta and S values, we see a very weak stabilization (Fig. 13). This is further confirmation that the shear is the dominant stabilization mechanism for the ideal mode. While the $n=1$ ideal mode is totally stabilized for $B_T/B_0 = 0.15$, the linear growth rate for the resistive mode is hardly modified.

The linear growth rate of a resistive instability is not, however, a good measure of its potential damaging effects to the plasma. For a resistive instability, it is necessary to study the nonlinear saturated level to have a relevant measure of the instability. The large aspect ratio of Heliotron E makes the straight approximation quite reasonable²¹ (Fig. 13). This approximation greatly simplifies the nonlinear calculations.

It is interesting to study the nonlinear 1/1 resistive instability below the ideal MHD threshold, because this is the regime relevant for the experiment. Therefore, we consider fixed $\beta_0 = 1.53\%$ equilibria with different values of added toroidal field B_T . For those equilibria, the ($m=1;n=1$) linear growth rate for $S = 10^5$ is practically independent of B_T . It goes from $\gamma = 1.09 \times 10^{-2} \tau_{hp}$ for $B_T = 0$, to $\gamma = 0.94 \times 10^{-2} \tau_{hp}$ for $B_T/B_0 = 0.15$. However, the nonlinear saturation level for the pressure fluctuation is clearly different. In Fig. 15 the nonlinear evolution of

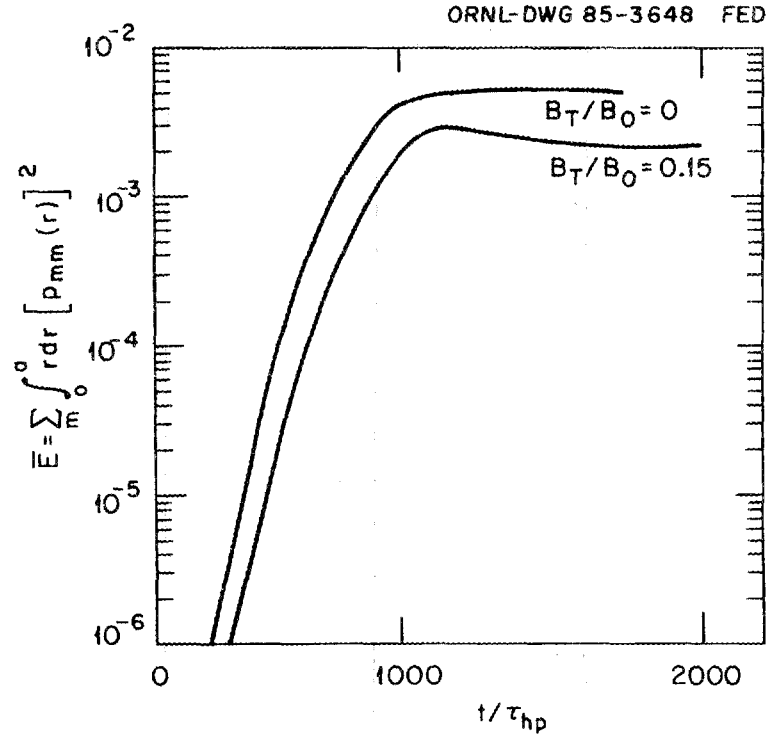


FIG. 15. Nonlinear evolution of the pressure fluctuations with and without additional toroidal field.

$$\bar{E} = \sum_m \int_0^a r dr (\tilde{p}_{mn}(r))^2$$

has been plotted. Here, \tilde{p}_{mn} is the $(m;n)$ Fourier component of the perturbed pressure. Therefore, \bar{E} is the rms value of the pressure fluctuation, which, for practical purposes, can be interpreted as the rms value of the density fluctuation. We can see that in the linear regime the evolution of \bar{E} is similar for both equilibria. However, in the case of added toroidal field the nonlinearities affect the evolution at a lower fluctuation level, and the saturation level is a factor of about 2.5 below the case without the additional toroidal field. In conclusion, the shear stabilization effects, which are weak for the linear resistive instability, have a stronger effect on the nonlinear saturated level of the instability. The added toroidal field is thus expected to have an effect on improving confinement for the Heliotron E plasmas at high beta.

VI. CONCLUSIONS

The dominant fixed-boundary $n=1$ instabilities in Heliotron E plasmas are interchange modes. Due to the nature of these modes, the marginal beta calculations require detailed convergence studies with radial grids finer than $\Delta\rho = 10^{-2}$. The stability properties depend strongly on the pressure profile. They are also sensitive to the transform profile, and the stability results are different for zero-current or flux-conserving equilibria. The former have more favorable stability properties with clear beta self-stabilization. The self-stabilization effect is due to increased shear at the $r=1$ surface, instead of the deepening of the magnetic well. Since zero-current equilibria are more stable, slow increases in the heating power could be expected to improve the chances of accessing high beta in Heliotron E. Because the nonlinear resistive stability also improves under those circumstances, better confinement can also be expected.

The addition of a relatively small toroidal field of about 5 to 15% of the total toroidal field greatly increases the flexibility of the device. Combining this added toroidal field with slow heating, the Heliotron E plasmas could gain stable access to the second stability region. In this way, average beta values of about 5% could be achieved.

The test of such predictions would be very important for the validation of the present techniques of calculating equilibrium and stability. The test is also important because if these results are correct, they show the existence of a new degree of freedom in designing a new device, the additional toroidal field. This makes the choice of number of toroidal field periods and aspect ratio of an optimal configuration less critical.

ACKNOWLEDGMENTS

One of us (B. A. Carreras) would like to thank Professor K. Uo and Professor A. Iiyoshi for their hospitality at the Plasma Physics Laboratory at Kyoto University during the summer of 1985, where part of this work was done. We also thank Professor O. Motojima for suggesting the inclusion of the toroidal field coils in the studies of Heliotron E stability and Dr. K. Hanatani for providing the information on the vacuum field configuration. We are particularly grateful to Professor M. Wakatani for many useful discussions, his help with the use of computer facilities at the Laboratory, and his continuous encouragement and support. We also extend thanks to Dr. J. Harris for useful suggestions and discussions.

REFERENCES

- ¹L. M. Kovrizhnykh and S. V. Shchepetov, *Sov. J. Plasma Phys.* 6, 533 (1980).
- ²B. A. Carreras, H. R. Hicks, J. A. Holmes, V. E. Lynch, L. Garcia, J. H. Harris, T. C. Hender, and B. F. Masden, *Phys. Fluids* 26, 3569 (1983).
- ³B. A. Carreras, H. R. Hicks, J. A. Holmes, V. E. Lynch, and G. H. Neilson, *Nucl. Fusion* 24, 1347 (1984).
- ⁴J. F. Lyon, B. A. Carreras, J. H. Harris, J. A. Rome, et al., in Proceedings of the 9th International Conference on Plasma Physics and Controlled Nuclear Fusion Research, Baltimore 1982, IAEA, Vienna, 1983, Vol. 3, p. 141.
- ⁵K. Uo, *J. Phys. Soc. Jpn.* 16, 1380 (1961).
- ⁶K. Uo, *Plasma Phys.* 13, 243 (1971).
- ⁷M. Wakatani, *IEEE Trans. Plasma Science* PA-9, 243 (1981).
- ⁸H. R. Strauss and D. A. Monticello, *Phys. Fluids* 24, 1148 (1981).
- ⁹G. Anania and J. L. Johnson, *Phys. Fluids* 26, 3070 (1983).
- ¹⁰F. Bauer, O. Betancourt, and P. Garabedian, *Phys. Fluids* 24, 48 (1981).
- ¹¹J. H. Harris, O. Motojima, P. Kaneko, S. Besshou, H. Zushi, M. Wakatani, F. Sano, S. Sudo, A. Sasaki, K. Kondo, M. Sato, T. Mutoh, T. Mizuuchi, M. Iima, T. Obiki, A. Iiyoshi, and K. Uo, *Phys. Rev. Lett.* 53, 2242 (1984).
- ¹²K. Uo, M. Nakasuga, and K. Hanatani, Heliotron Magnetic Surfaces, Report PPLK-3, Plasma Physics Laboratory, Kyoto University, 1982.
- ¹³J. M. Greene and J. L. Johnson, *Phys. Fluids* 4, 875 (1961).
- ¹⁴F. Herrnegger, P. Merkel, and J. L. Johnson, Comparison of Two Dimensional and Three Dimensional MHD Equilibria and Stability Codes, to be published.
- ¹⁵J. A. Holmes, Y-K. M. Peng, S. J. Lynch, *J. Comput. Phys.* 36, 35 (1980).
- ¹⁶H. R. Strauss, *Plasma Phys.* 22, 733 (1980).
- ¹⁷L. Charlton, B. A. Carreras, J. A. Holmes, H. R. Hicks, and V. E. Lynch, to be published in *J. Comput. Phys.*

- ¹⁸V. E. Lynch, B. A. Carreras, L. A. Charlton, T. C. Hender, L. Garcia, H. R. Hicks, and J. A. Holmes, Stellarator Expansion Methods for MHD Equilibrium and Stability Calculations, Report ORNL/TM-9861, Oak Ridge National Laboratory, 1985.
- ¹⁹M. Wakatani (private communication).
- ²⁰F. Bauer, O. Betancourt, and P. Garabedian, Magnetohydrodynamic Equilibrium and Stability of Stellarators (Springer-Verlag, New York, 1986).
- ²¹M. Wakatani, H. Shirai, and M. Yamagiwa, Nucl. Fusion 24, 1407 (1984).

INTERNAL DISTRIBUTION

- | | | | |
|--------|-------------------|--------|---|
| 1. | L. A. Berry | 21. | J. F. Lyon |
| 2-6. | B. A. Carreras | 22. | M. M. Murakami |
| 7. | L. A. Charlton | 23. | Y-K. M. Peng |
| 8. | R. A. Dory | 24. | J. A. Rome |
| 9. | J. Dunlap | 25. | J. Sheffield |
| 10-11. | L. Garcia | 26-27. | Laboratory Records Department |
| 12. | J. H. Harris | 28. | Laboratory Records, ORNL-RC |
| 13. | H. Haselton | 29. | Document Reference Section |
| 14. | P. N. Haubenreich | 30. | Central Research Library |
| 15. | C. L. Hedrick | 31. | Fusion Energy Division Library |
| 16. | J. T. Hogan | 32. | Fusion Energy Division Publications
Office |
| 17. | J. A. Holmes | 33. | ORNL Patent Office |
| 18. | M. S. Lubell | | |
| 19-20. | V. E. Lynch | | |

EXTERNAL DISTRIBUTION

34. M. Wakatani, Plasma Physics Laboratory, Kyoto University, Gokasho, Uji, Japan
35. O. Motojima, Plasma Physics Laboratory, Kyoto University, Gokasho, Uji, Japan
36. J. L. Johnson, Princeton Plasma Physics Laboratory, Princeton University, P.O. Box 451, Princeton, NJ 08544
37. Office of the Assistant Manager for Energy Research and Development, U.S. Department of Energy, Oak Ridge Operations Office, P.O. Box E, Oak Ridge, TN 37831
38. J. D. Callen, Department of Nuclear Engineering, University of Wisconsin, Madison, WI 53706
39. R. W. Conn, Department of Chemical, Nuclear, and Thermal Engineering, University of California, Los Angeles, CA 90024
40. S. O. Dean, Director, Fusion Energy Development, Science Applications, Inc., 2 Professional Drive, Suite 249, Gaithersburg, MD 20760
41. H. K. Forsen, Bechtel Group, Inc., Research Engineering, P.O. Box 3965, San Francisco, CA 94105
42. J. R. Gilleland, GA Technologies, Inc., Fusion and Advanced Technology, P.O. Box 85608, San Diego, CA 92138
43. R. W. Gould, Department of Applied Physics, California Institute of Technology, Pasadena, CA 91125
44. R. A. Gross, Plasma Research Library, Columbia University, New York, NY 10027
45. D. M. Meade, Princeton Plasma Physics Laboratory, P.O. Box 451, Princeton, NJ 08544

46. P. J. Reardon, Brookhaven National Laboratory, Upton, NY 11973
47. M. Roberts, International Programs, Office of Fusion Energy, Office of Energy Research, ER-52, U.S. Department of Energy, Washington, DC 20545
48. W. M. Stacey, Fusion Research Center, Emerson-Cherry Bldg., Georgia Institute of Technology, Atlanta, GA 30332
49. D. Steiner, Nuclear Engineering Department, NES Building, Tibbetts Avenue, Rensselaer Polytechnic Institute, Troy, NY 12181
50. R. Varma, Physical Research Laboratory, Navrangpura, Ahmedabad 380009, India
51. Bibliothek, Max-Planck Institut fur Plasmaphysik, D-8046 Garching bei Munchen, Federal Republic of Germany
52. Bibliothek, Institut fur Plasmaphysik, KFA, Postfach 1913, D-5170 Julich, Federal Republic of Germany
53. Bibliotheque, Centre des Recherches en Physique des Plasmas, 21 Avenue des Bains, 1007 Lausanne, Switzerland
54. Bibliotheque, Service du Confinement des Plasmas, CEA, B.P. No. 6, 92 Fontenay-aux-Roses (Seine), France
55. Documentation S.I.G.N., Departement de la Physique du Plasma et de la Fusion Controlee, Centre d'Etudes Nucleaires, B.P. 85, Centre du Tri, 38081 Cedex, Grenoble, France
56. Library, Culham Laboratory, UKAEA, Abingdon, Oxfordshire, OX14 3DB, England
57. Library, FOM-Instituut voor Plasma-Fysica, Rijnhuizen, Edisonbaan 14, 3439 MN Nieuwegein, The Netherlands
58. Library, Institute of Plasma Physics, Nagoya University, Nagoya 464, Japan
59. Library, International Centre for Theoretical Physics, Trieste, Italy
60. Library, Laboratorio Gas Ionizzati, CP 56, I-00044 Frascati, Rome, Italy
61. Library, Plasma Physics Laboratory, Kyoto University, Gokasho, Uji, Kyoto, Japan
62. Plasma Research Laboratory, Australian National University, P.O. Box 4, Canberra, A.C.T. 2000, Australia
63. Thermonuclear Library, Japan Atomic Energy Research Institute, Tokai-mura, Ibaraki Prefecture, Japan
64. G. A. Eliseev, I. V. Kurchatov Institute of Atomic Energy, P.O. Box 3402, 123182 Moscow, U.S.S.R.
65. V. A. Glukhikh, Scientific-Research Institute of Electro-Physical Apparatus, 188631 Leningrad, U.S.S.R.
66. I. Shpigel, Institute of General Physics, U.S.S.R. Academy of Sciences, Ulitsa Vavilova 38, Moscow, U.S.S.R.
67. D. D. Ryutov, Institute of Nuclear Physics, Siberian Branch of the Academy of Sciences of the U.S.S.R., Sovetskaya St. 5, 630090 Novosibirsk, U.S.S.R.
68. V. T. Tolok, Kharkov Physical-Technical Institute, Academical St. 1, 310108 Kharkov, U.S.S.R.
69. Library, Institute of Physics, Academia Sinica, P.O. Box 3908, Beijing, Peoples Republic of China
70. J. F. Clarke, Associate Director for Fusion Energy, Office of Fusion Energy, ER-50, Germantown, U.S. Department of Energy, Washington, DC 20545
71. N. A. Davies, Office of the Associate Director, Office of Fusion Energy, Office of Energy Research, ER-51, Germantown, U.S. Department of Energy, Washington, DC 20545

72. D. B. Nelson, Director, Division of Applied Plasma Physics, Office of Fusion Energy, Office of Energy Research, ER-54, Germantown, U.S. Department of Energy, Washington, DC 20545
73. E. Oktay, Division of Confinement Systems, Office of Fusion Energy, Office of Energy Research, ER-55, Germantown, U.S. Department of Energy, Washington, DC 20545
74. A. L. Opdenaker, Fusion Systems Design Branch, Division of Development and Technology, Office of Fusion Energy, Office of Energy Research, ER-532, Germantown, U.S. Department of Energy, Washington, DC 20545
75. W. Sadowski, Fusion Theory and Computer Services Branch, Division of Applied Plasma Physics, Office of Fusion Energy, Office of Energy Research, ER-541, Germantown, U.S. Department of Energy, Washington, DC 20545
76. P. M. Stone, Fusion Systems Design Branch, Division of Development and Technology, Office of Fusion Energy, Office of Energy Research, ER-532, Germantown, U.S. Department of Energy, Washington, DC 20545
77. J. M. Turner, International Programs, Office of Fusion Energy, Office of Energy Research, ER-52, Germantown, U.S. Department of Energy, Washington, DC 20545
78. R. E. Mickens, Atlanta University, Department of Physics, Atlanta, GA 30314
79. M. N. Rosenbluth, RLM 11.218, Institute for Fusion Studies, University of Texas, Austin, TX 78712
80. Theory Department Read File, c/o D. W. Ross, University of Texas, Institute for Fusion Studies, Austin, TX 78712
81. Theory Department Read File, c/o R. C. Davidson, Director, Plasma Fusion Center, NW 16-202, Massachusetts Institute of Technology, Cambridge, MA 02139
82. Theory Department Read File, c/o F. W. Perkins, Princeton Plasma Physics Laboratory, P.O. Box 451, Princeton, NJ 08544
83. Theory Department Read File, c/o L. Kovrizhnykh, Institute of General Physics, U.S.S.R. Academy of Sciences, Ulitsa Vavilova 38, Moscow, U.S.S.R.
84. Theory Department Read File, c/o B. B. Kadomtsev, I. V. Kurchatov Institute of Atomic Energy, P.O. Box 3402, 123182 Moscow, U.S.S.R.
85. Theory Department Read File, c/o T. Kamimura, Institute of Plasma Physics, Nagoya University, Nagoya 464, Japan
86. Theory Department Read File, c/o C. Mercier, Euratom-CEA, Service des Recherches sur la Fusion Controlee, Fontenay-aux-Roses (Seine), France
87. Theory Department Read File, c/o T. E. Stringer, JET Joint Undertaking, Culham Laboratory, Abingdon, Oxfordshire OX14 3DB, England
88. Theory Department Read File, c/o K. Roberts, Culham Laboratory, Abingdon, Oxfordshire OX14 3DB, England
89. Theory Department Read File, c/o D. Biskamp, Max-Planck-Institut fur Plasmaphysik, D-8046 Garching bei Munchen, Federal Republic of Germany
90. Theory Department Read File, c/o T. Takeda, Japan Atomic Energy Research Institute, Tokai-mura, Ibaraki Prefecture, Japan
91. Theory Department Read File, c/o C. S. Liu, GA Technologies, Inc., P.O. Box 81608, San Diego, CA 92138
92. Theory Department Read File, c/o L. D. Pearlstein, Lawrence Livermore National Laboratory, P.O. Box 808, Livermore, CA 94550

93. Theory Department Read File, c/o R. Gerwin, CTR Division, Los Alamos National Laboratory, P.O. Box 1663, Los Alamos, NM 87545
 94. C. De Palo, Library, Associazione EURATOM-ENEA sulla Fusione, CP 65, I-00044 Frascati (Roma), Italy
 95. H. Weitzner, Courant Institute of Mathematical Sciences, New York University, New York, NY 10012
- 96--247. Given distribution as shown in TIC-4500, Magnetic Fusion Energy (Category UC-20g, Theoretical Plasma Physics)